Measurements of the b̄b production cross section and forward–backward asymmetry at centre-of-mass energies above the Z pole at LEP

L3 Collaboration

M. Acciarri [z], P. Achard [s], O. Adriani [p], M. Aguilar-Benitez [y],
J. Alcaraz [y], G. Alemanni [v], J. Allaby [q], A. Aloisio [ab], M.G. Alviggi [ab], G. Ambrosi [s],
H. Anderhub [av], V.P. Andreev [f,aj], T. Angelescu [l], F. Anselmo [i], A. Arefiev [aa],
T. Azemoon [c], T. Aziz [j], P. Bagnaia [ai], A. Bajo [y], L. Baksay [aq], A. Balandras [d],
S.V. Baldew [b], S. Banerjee [j], Sw. Banerjee [j], A. Barczyk [av,at], R. Barillère [q],
L. Barone [ai], P. Bartalini [v], M. Basile [i], R. Battiston [af], A. Bay [v], F. Becattini [p],
U. Becker [n], F. Behner [av], L. Bellucci [p], R. Berbeco [c], J. Berdugo [y], P. Berges [n],
B. Bertucci [af], B.L. Betev [av], S. Bhattacharya [j], M. Biasini [af], A. Biland [av],
J.J. Blaising [d], S.C. Blyth [ag], G.J. Bobbink [b], A. Böhm [a],
L. Boldizsar [m], B. Borgia [ai], D. Bourilkov [av], M. Bourquin [s],
S. Braccini [s], J.G. Branson [am], V. Brigljevic [av], F. Brochu [d], A. Buffini [p], A. Buijs [ar],
J.D. Burger [n], W.J. Burger [af], X.D. Cai [n], M. Campanelli [av], M. Capell [n],
G. Cara Romeo [i], G. Carlino [ab], A.M. Cartacci [p], J. Casaus [y], G. Castellini [p],
F. Cavallari [ai], N. Cavallo [ak], C. Cecchi [af], M. Cerrada [y], F. Cesaroni [w], M. Chamizo [s],
Y.H. Chang [ax], U.K. Chaturvedi [r], M. Chemarin [x], A. Chen [ax], G. Chen [g], G.M. Chen [g],
H.F. Chen [t], H.S. Chen [g], G. Chiefari [ab], L. Cifarelli [al], F. Cindolo [i], C. Civinini [p],
I. Clare [n], R. Clare [n], G. Coignet [d], N. Colino [y], S. Costantini [e], F. Cotorobai [l],
B. Cozzoni [i], B. de la Cruz [y], A. Csilling [m], S. Cucciarelli [af], T.S. Dai [n],
J.A. van Dalen [ad], R. D'Alessandro [p], R. de Asmundis [ab], P. Déglon [s], A. Degré [d],
K. Deiters [at], D. della Volpe [ab], E. Delmeire [s], P. Denes [ah], F. DeNotaristefani [ai],
A. De Salvo [av], M. Diemoz [ai], M. Dierckxsens [b], D. van Dierendonck [b],
F. Di Lodovico [av], C. Dionisi [ai], M. Dittmar [av], A. Dominguez [am], A. Doria [ab],
M.T. Dova [r,5], D. Duchesneau [d], D. Dufournaud [d], P. Duinker [b], I. Duran [an],
H. El Mamouni [x], A. Engler [ag], F.J. Eppling [n], F.C. Erné [b], P. Extermann [s], M. Fabre [at],
R. Faccini [ai], M.A. Falagan [y], S. Falciano [ai,q], A. Favara [q], J. Fay [x], O. Fedin [aj],

M. Felcini [av], T. Ferguson [ag], F. Ferroni [ai], H. Fesefeldt [a], E. Fiandrini [af], J.H. Field [s],
F. Filthaut [q], P.H. Fisher [n], I. Fisk [am], G. Forconi [n], K. Freudenreich [av], C. Furetta [z],
Yu. Galaktionov [aa,n], S.N. Ganguli [j], P. Garcia-Abia [e], M. Gataullin [ae], S.S. Gau [k],
S. Gentile [ai,q], N. Gheordanescu [l], S. Giagu [ai], Z.F. Gong [t], G. Grenier [x],
O. Grimm [av], M.W. Gruenewald [h], M. Guida [al], R. van Gulik [b], V.K. Gupta [ah],
A. Gurtu [j], L.J. Gutay [as], D. Haas [e], A. Hasan [ac], D. Hatzifotiadou [i], T. Hebbeker [h],
A. Hervé [q], P. Hidas [m], J. Hirschfelder [ag], H. Hofer [av], G. Holzner [av], H. Hoorani [ag],
S.R. Hou [ax], Y. Hu [ad], I. Iashvili [au], B.N. Jin [g], L.W. Jones [c], P. de Jong [b],
I. Josa-Mutuberría [y], R.A. Khan [r], M. Kaur [r,6], M.N. Kienzle-Focacci [s], D. Kim [ai],
J.K. Kim [ap], J. Kirkby [q], D. Kiss [m], W. Kittel [ad], A. Klimentov [n,aa], A.C. König [ad],
A. Kopp [au], V. Koutsenko [n,aa], M. Kräber [av], R.W. Kraemer [ag], W. Krenz [a],
A. Krüger [au], A. Kunin [n,aa], P. Ladron de Guevara [y], I. Laktineh [x], G. Landi [p],
K. Lassila-Perini [av], M. Lebeau [q], A. Lebedev [n], P. Lebrun [x], P. Lecomte [av], P. Lecoq [q],
P. Le Coultre [av], H.J. Lee [h], J.M. Le Goff [q], R. Leiste [au], E. Leonardi [ai],
P. Levtchenko [aj], C. Li [t], S. Likhoded [au], C.H. Lin [ax], W.T. Lin [ax], F.L. Linde [b],
L. Lista [ab], Z.A. Liu [g], W. Lohmann [au], E. Longo [ai], Y.S. Lu [g], K. Lübelsmeyer [a],
C. Luci [q,ai], D. Luckey [n], L. Lugnier [x], L. Luminari [ai], W. Lustermann [av], W.G. Ma [t],
M. Maity [j], L. Malgeri [q], A. Malinin [q], C. Maña [y], D. Mangeol [ad], J. Mans [ah],
P. Marchesini [av], G. Marian [o], J.P. Martin [x], F. Marzano [ai], K. Mazumdar [j],
R.R. McNeil [f], S. Mele [q], L. Merola [ab], M. Meschini [p], W.J. Metzger [ad],
M. von der Mey [a], A. Mihul [l], H. Milcent [q], G. Mirabelli [ai], J. Mnich [q],
G.B. Mohanty [j], P. Molnar [h], B. Monteleoni [p,8], T. Moulik [j], G.S. Muanza [x],
A.J.M. Muijs [b], M. Musy [ai], M. Napolitano [ab], F. Nessi-Tedaldi [av], H. Newman [ae],
T. Niessen [a], A. Nisati [ai], H. Nowak [au], G. Organtini [ai], A. Oulianov [aa], C. Palomares [y],
D. Pandoulas [a], S. Paoletti [ai,q], P. Paolucci [ab], R. Paramatti [ai], H.K. Park [ag], I.H. Park [ap],
G. Passaleva [q], S. Patricelli [ab], T. Paul [k], M. Pauluzzi [af], C. Paus [q], F. Pauss [av],
M. Pedace [ai], S. Pensotti [z], D. Perret-Gallix [d], B. Petersen [ad], D. Piccolo [ab], F. Pierella [i],
M. Pieri [p], P.A. Piroué [ah], E. Pistolesi [z], V. Plyaskin [aa], M. Pohl [s], V. Pojidaev [aa,p],
H. Postema [n], J. Pothier [q], D.O. Prokofiev [as], D. Prokofiev [aj], J. Quartieri [al],
G. Rahal-Callot [av,q], M.A. Rahaman [j], P. Raics [o], N. Raja [j], R. Ramelli [av],
P.G. Rancoita [z], A. Raspereza [au], G. Raven [am], P. Razis [ac], D. Ren [av], M. Rescigno [ai],
S. Reucroft [k], S. Riemann [au], K. Riles [c], A. Robohm [av], J. Rodin [aq], B.P. Roe [c],
L. Romero [y], A. Rosca [h], S. Rosier-Lees [d], J.A. Rubio [q], G. Ruggiero [p],
D. Ruschmeier [h], H. Rykaczewski [av], S. Saremi [f], S. Sarkar [ai],
J. Salicio [q], E. Sanchez [q], M.P. Sanders [ad], M.E. Sarakinos [u],
C. Schäfer [q], V. Schegelsky [aj], S. Schmidt-Kaerst [a],
D. Schmitz [a], H. Schopper [aw], D.J. Schotanus [ad], G. Schwering [a], C. Sciacca [ab],
D. Sciarrino [s], A. Seganti [i], L. Servoli [af], S. Shevchenko [ae], N. Shivarov [ao],

V. Shoutko [aa], E. Shumilov [aa], A. Shvorob [ae], T. Siedenburg [a], D. Son [ap], B. Smith [ag],
P. Spillantini [p], M. Steuer [n], D.P. Stickland [ah], A. Stone [f], B. Stoyanov [ao],
A. Straessner [a], K. Sudhakar [j], G. Sultanov [r], L.Z. Sun [t], H. Suter [av], J.D. Swain [r],
Z. Szillasi [aq,3], T. Sztaricskai [aq,3], X.W. Tang [g], L. Tauscher [e], L. Taylor [k], B. Tellili [x],
C. Timmermans [ad], Samuel C.C. Ting [n], S.M. Ting [n], S.C. Tonwar [j], J. Tóth [m],
C. Tully [q], K.L. Tung [g], Y. Uchida [n], J. Ulbricht [av], E. Valente [ai], G. Vesztergombi [m],
I. Vetlitsky [aa], D. Vicinanza [al], G. Viertel [av], S. Villa [k], M. Vivargent [d], S. Vlachos [e],
I. Vodopianov [aj], H. Vogel [ag], H. Vogt [au], I. Vorobiev [aa], A.A. Vorobyov [aj],
A. Vorvolakos [ac], M. Wadhwa [e], W. Wallraff [a], M. Wang [n], X.L. Wang [t], Z.M. Wang [t],
A. Weber [a], M. Weber [a], P. Wienemann [a], H. Wilkens [ad], S.X. Wu [n], S. Wynhoff [q],
L. Xia [ae], Z.Z. Xu [t], J. Yamamoto [c], B.Z. Yang [t], C.G. Yang [g], H.J. Yang [g], M. Yang [g],
J.B. Ye [t], S.C. Yeh [ay], An. Zalite [aj], Yu. Zalite [aj], Z.P. Zhang [t], G.Y. Zhu [g], R.Y. Zhu [ae],
A. Zichichi [i,q,r], G. Zilizi [aq,3], M. Zöller [a]

[a] *I. Physikalisches Institut, RWTH, D-52056 Aachen, Germany,*
and III. Physikalisches Institut, RWTH, D-52056 Aachen, Germany [1]
[b] *National Institute for High Energy Physics, NIKHEF, and University of Amsterdam, NL-1009 DB Amsterdam, The Netherlands*
[c] *University of Michigan, Ann Arbor, MI 48109, USA*
[d] *Laboratoire d'Annecy-le-Vieux de Physique des Particules, LAPP, IN2P3-CNRS, BP 110, F-74941 Annecy-le-Vieux CEDEX, France*
[e] *Institute of Physics, University of Basel, CH-4056 Basel, Switzerland*
[f] *Louisiana State University, Baton Rouge, LA 70803, USA*
[g] *Institute of High Energy Physics, IHEP, 100039 Beijing, China* [7]
[h] *Humboldt University, D-10099 Berlin, Germany* [1]
[i] *University of Bologna and INFN-Sezione di Bologna, I-40126 Bologna, Italy*
[j] *Tata Institute of Fundamental Research, Bombay 400 005, India*
[k] *Northeastern University, Boston, MA 02115, USA*
[l] *Institute of Atomic Physics and University of Bucharest, R-76900 Bucharest, Romania*
[m] *Central Research Institute for Physics of the Hungarian Academy of Sciences, H-1525 Budapest 114, Hungary* [2]
[n] *Massachusetts Institute of Technology, Cambridge, MA 02139, USA*
[o] *KLTE-ATOMKI, H-4010 Debrecen, Hungary* [3]
[p] *INFN Sezione di Firenze and University of Florence, I-50125 Florence, Italy*
[q] *European Laboratory for Particle Physics, CERN, CH-1211 Geneva 23, Switzerland*
[r] *World Laboratory, FBLJA Project, CH-1211 Geneva 23, Switzerland*
[s] *University of Geneva, CH-1211 Geneva 4, Switzerland*
[t] *Chinese University of Science and Technology, USTC, Hefei, Anhui 230 029, China* [7]
[u] *SEFT, Research Institute for High Energy Physics, P.O. Box 9, SF-00014 Helsinki, Finland*
[v] *University of Lausanne, CH-1015 Lausanne, Switzerland*
[w] *INFN-Sezione di Lecce and Universitá Degli Studi di Lecce, I-73100 Lecce, Italy*
[x] *Institut de Physique Nucléaire de Lyon, IN2P3-CNRS, Université Claude Bernard, F-69622 Villeurbanne, France*
[y] *Centro de Investigaciones Energéticas, Medioambientales y Tecnologícas, CIEMAT, E-28040 Madrid, Spain* [4]
[z] *INFN-Sezione di Milano, I-20133 Milan, Italy*
[aa] *Institute of Theoretical and Experimental Physics, ITEP, Moscow, Russia*
[ab] *INFN-Sezione di Napoli and University of Naples, I-80125 Naples, Italy*
[ac] *Department of Natural Sciences, University of Cyprus, Nicosia, Cyprus*
[ad] *University of Nijmegen and NIKHEF, NL-6525 ED Nijmegen, The Netherlands*
[ae] *California Institute of Technology, Pasadena, CA 91125, USA*
[af] *INFN-Sezione di Perugia and Universitá Degli Studi di Perugia, I-06100 Perugia, Italy*
[ag] *Carnegie Mellon University, Pittsburgh, PA 15213, USA*
[ah] *Princeton University, Princeton, NJ 08544, USA*
[ai] *INFN-Sezione di Roma and University of Rome, ''La Sapienza'', I-00185 Rome, Italy*
[aj] *Nuclear Physics Institute, St. Petersburg, Russia*
[ak] *INFN-Sezione di Napoli and University of Potenza, I-85100 Potenza, Italy*

al *University and INFN, Salerno, I-84100 Salerno, Italy*
am *University of California, San Diego, CA 92093, USA*
an *Dept. de Fisica de Particulas Elementales, Univ. de Santiago, E-15706 Santiago de Compostela, Spain*
ao *Bulgarian Academy of Sciences, Central Lab. of Mechatronics and Instrumentation, BU-1113 Sofia, Bulgaria*
ap *Laboratory of High Energy Physics, Kyungpook National University, 702-701 Taegu, South Korea*
aq *University of Alabama, Tuscaloosa, AL 35486, USA*
ar *Utrecht University and NIKHEF, NL-3584 CB Utrecht, The Netherlands*
as *Purdue University, West Lafayette, IN 47907, USA*
at *Paul Scherrer Institut, PSI, CH-5232 Villigen, Switzerland*
au *DESY, D-15738 Zeuthen, Germany*
av *Eidgenössische Technische Hochschule, ETH Zürich, CH-8093 Zürich, Switzerland*
aw *University of Hamburg, D-22761 Hamburg, Germany*
ax *National Central University, Chung-Li, Taiwan, ROC*
ay *Department of Physics, National Tsing Hua University, Taiwan, ROC*

Dedicated to the memory of Prof. Bianca Monteleoni.

Abstract

The measurements of $R_b = \sigma(e^+e^- \to b\bar{b})/\sigma(e^+e^- \to q\bar{q})$ and of the b quark forward–backward charge asymmetry, A_{fb}^b, at centre-of-mass energies above the Z pole are described. The measurement of R_b is performed at $\sqrt{s}$ between 130 and 189 GeV using a b-tagging method that exploits the relatively large decay length of b-hadrons. The measurement of A_{fb}^b is performed using the large statistics event sample collected at $\sqrt{s} = 189$ GeV with a lepton-tag analysis based on the selection of prompt muons and electrons. The results at $\sqrt{s} = 189$ GeV are $R_b = 0.163 \pm 0.013 \,(\text{stat.}) \pm 0.005 \,(\text{syst.})$, $A_{fb}^b = 0.61 \pm 0.18 \,(\text{stat.}) \pm 0.09 \,(\text{syst.})$. © 2000 Elsevier Science B.V. All rights reserved.

1. Introduction

The ratio $R_b = \sigma(e^+e^- \to b\bar{b})/\sigma(e^+e^- \to q\bar{q})$ and the bottom quark forward–backward asymmetry A_{fb}^b are important parameters in precision studies of the Standard Model [1] and are sensitive probes to new physics. Their values have been measured very precisely at the Z pole [2–6]. The measurements of these two quantities at centre-of-mass energies above the Z peak provide further tests of the Standard Model and put additional constraints on new physics, such as contact interactions [7].

In this paper the measurements of R_b at centre-of-mass energies between 130 and 189 GeV and of A_{fb}^b at $\sqrt{s} = 189$ GeV obtained with the L3 detector [8] at LEP are described. The main features that distinguish the production of $b\bar{b}$ pairs from lighter quark production are the long lifetime and hard fragmentation of b-flavoured hadrons and the large lepton momentum in semileptonic decays. The measurement of R_b is based on a b-tagging method using lifetime information which uses data taken with the L3 Silicon Microvertex Detector (SMD) [9]. The measurement of A_{fb}^b exploits the characteristic semileptonic decays of b-hadrons and relies on the good lepton identification and lepton energy resolution of the L3 detector. It requires leptons with high

momentum along and transverse to the direction of the associated jet, caused by the hard fragmentation and high mass of the decaying hadron. Similar measurements have been published by other LEP collaborations [10].

2. Event selection

The data analysed in this paper are those collected by L3 from 1995 to 1998 at centre-of-mass energies between 130 GeV and 189 GeV. As the integrated luminosity at 130 GeV and 136 GeV is small, the corresponding data are combined and a luminosity weighted average centre-of-mass energy of 133.2 GeV is used. The centre-of-mass energies and the corresponding integrated luminosities used in the analysis are summarised in Table 1.

The measurements of R_b and A_{fb}^b are performed using a sample of $e^+e^- \to Z^*/\gamma^* \to q\bar{q}(\gamma)$ events selected with criteria similar to those used for the measurement of the $e^+e^- \to$ hadrons cross section [11]. The signal events are required to have an effective centre-of-mass energy $\sqrt{s'} > 0.85\sqrt{s}$. This requirement rejects a large fraction of events with initial state radiation. Mis-reconstruction of the effective centre-of-mass energy induces a migration of radiative events to the kinematic region allowed by the cut on $\sqrt{s'}$. This is taken into account in the analysis as an additional background, called radiative background. No correction is applied to the final results to take into account the interference between initial- and final-state radiative corrections.

To further reject radiative events, the visible energy, E_{vis}, is required to be greater than $0.6\sqrt{s}$ and the longitudinal energy imbalance must be less than $0.25 E_{vis}$. The events are selected in a fiducial region defined by $|\cos\theta| < 0.85$, where θ is the polar angle of the thrust axis. This cut ensures good track quality and efficient lepton identification. For centre-of-mass

energies larger than the W-pair production threshold, additional cuts are needed to reject the W^+W^- background. To reject hadronic W decays, the variable y_{34} is required to be less than 0.011, where y_{34} is the Durham jet finding algorithm parameter [12] for which the transition from three to four jets occurs. As the W^+W^- background increases for higher centre-of-mass energies, the maximum allowed value of y_{34} is lowered to 0.008 at $\sqrt{s} = 183$ GeV and to 0.006 at 189 GeV. Furthermore, to reject semileptonic W decays, the transverse energy imbalance must be smaller than $0.4 E_{vis}$. For the A_{fb}^b analysis the presence of an identified electron or muon with an energy smaller than 40 GeV is required.

Efficiency and background studies are performed for each centre-of-mass energy using the following event generators: PYTHIA [13] ($e^+e^- \to$ hadrons(γ), Zee), KORALZ [14] ($\tau^+\tau^-(\gamma)$), PHOJET [15] (hadronic two-photon collisions), KORALW [16] ($e^+e^- \to W^+W^-(\gamma)$) and EXCALIBUR [17] ($e^+e^- \to q\bar{q}q'\bar{q}'$), which includes the ZZ production diagrams.

3. Measurement of R_b

The measurement of R_b is based on a b-tagging algorithm that exploits the relatively large decay length of b-hadrons [18]. The confidence level, C_N, that a set of N tracks originated from the primary vertex, is constructed using the decay length significance L/σ_L of each track. First the crossing point of each track with the closest jet is determined in both the $r\phi$ and sz projections. Then the signed distances ($d_{r\phi}$, d_{sz}) between these crossing points and the reconstructed primary event vertex are projected onto the jet axis to determine the decay length, L. If the probability that both $r\phi$ and sz measurements are compatible exceeds 5%, then the two are combined. Otherwise, only the $r\phi$ projection is used.

Small biases in $d_{r\phi}$ and d_{sz} are removed by recalibrating their mean values as functions of the azimuthal and polar angles of the tracks. The errors on $d_{r\phi}$ and d_{sz} are parametrised to take into account the contributions coming from the track fit, the primary vertex position measurement and the effect

Table 1
Summary of centre-of-mass energies and integrated luminosities considered in this analysis

$\sqrt{s}$ (GeV)	133.2	161.3	172.1	182.7	188.6
$\mathscr{L}$ (pb^{-1})	12.01	10.95	10.25	55.65	176.3

of multiple scattering. The estimated errors on $d_{r\phi}$ and d_{sz} are rescaled by comparing their values with those observed in a sample of tracks with negative decay length. The scale factors are found to be within 10% of unity. The tracking resolution depends critically on the pattern of SMD hits associated to the tracks. Therefore the tracks are grouped into different classes according to the vertex detector hit pattern and for each class different resolution parameters are considered. The study of the tracking resolution described above is performed using samples of hadronic Z decays corresponding to an integrated luminosity of about $2.5 \, \text{pb}^{-1}$ each, collected each year during calibration runs at the Z peak.

The confidence level, C_N, is calculated by taking into account the fraction of tracks with positive decay length,

$$C_N = \frac{\Pi}{2^N} \sum_{i=0}^{N-1} \sum_{j=i+1}^{N} \binom{N}{j} \frac{(-\log \Pi)^i}{i!} ,$$

$$\Pi = \prod_{k=1}^{N_+} P_k(L/\sigma_L), \qquad (1)$$

where N_+ is the number of tracks with positive decay length. The probability that a track originated from the primary vertex, $P(L/\sigma_L)$, is obtained by fitting the distribution of the decay length signifi-
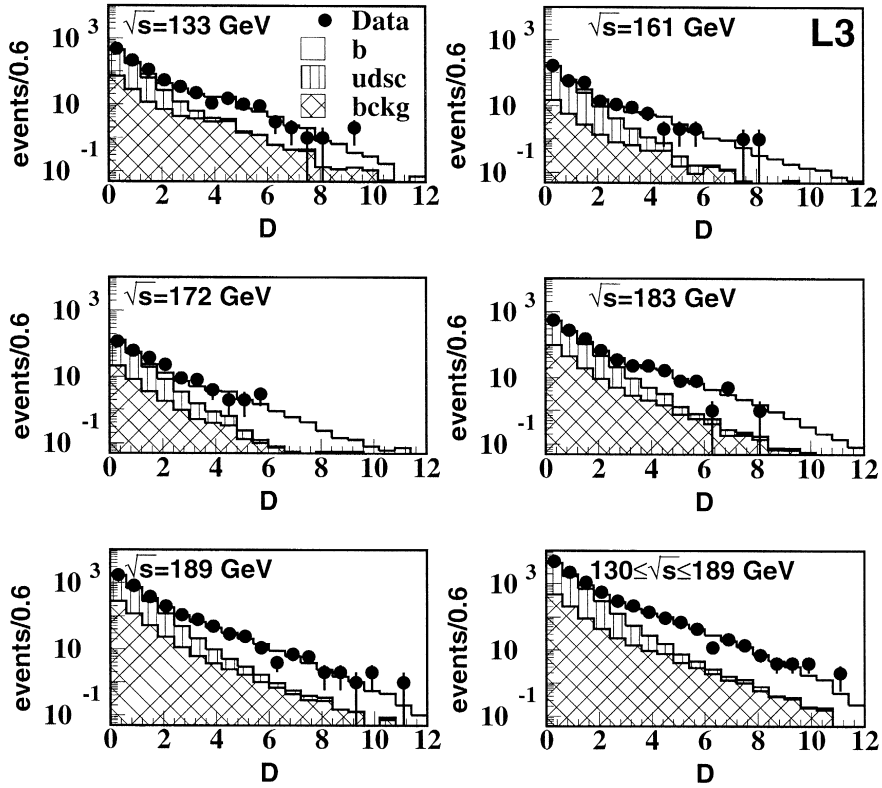
Fig. 1. Distributions of the b-tagging discriminant for the selected events at the different centre-of-mass energies. The points are the data and the solid lines represent the total Monte Carlo expectation. The open histograms show the signal contribution, the vertically hatched histograms represent the c and light quark background from q$\bar{\text{q}}$ events and the cross-hatched histograms represent the sum of non-q$\bar{\text{q}}$ and radiative background, as indicated in the legend of the upper left figure. In the bottom right plot, the distribution for the total selected sample is shown.

Table 2
Values of R_c^{SM} used for the measurement of R_b and coefficients $a(R_c)$ giving the dependence of the measured R_b on R_c (Eq. (3))

$\sqrt{s}$ (GeV)	133	161	172	183	189
R_c^{SM}	0.221	0.242	0.246	0.250	0.252
$a(R_c)$	-0.113	-0.118	-0.106	-0.099	-0.100

cance for tracks with negative decay length. The shape of this distribution is due to detector resolution effects and is modelled by a resolution function parametrised as the sum of two gaussians and an exponential tail. The distributions of the discriminant variable $D = -\log_{10}(C_N)$ obtained at the different centre-of-mass energies are shown in Fig. 1.

The measurement of R_b is performed using an event-tag method by counting the events containing b quarks. The b-events are selected by applying a cut on the discriminant where the cut position is chosen so that the expected statistical error on the cross section $\sigma(e^+e^- \to b\bar{b})$ is minimised. Given the num-

ber N_t^{obs} of tagged events and N_t^{bkg} of tagged background events, R_b is derived from the formula:

$$R_b = \frac{1}{\varepsilon_b - \varepsilon_{uds}} \left[\frac{N_t^{obs} - N_t^{bkg}}{N^{obs} - N^{bkg}} - \varepsilon_c R_c - \varepsilon_{uds}(1 - R_c) \right], \quad (2)$$

where N^{obs} and N^{bkg} are respectively the total number of selected $q\bar{q}$ events in data and the total number of background events from Monte Carlo; ε_b, ε_c and ε_{uds} are the tagging efficiencies for b, c and light quarks, respectively, and are estimated from Monte Carlo.

The value of the $c\bar{c}$ production cross section, R_c, is taken from the Standard Model prediction calculated by ZFITTER [19]. The dependence of R_b on R_c can be parametrised as

$$\Delta R_b = a(R_c)\,\Delta R_c, \quad (3)$$

where $\Delta R_c = R_c - R_c^{SM}$. The values of R_c^{SM} used in the measurement and the corresponding coefficients $a(R_c)$ are shown in Table 2.

Table 3
Number of selected (N^{obs}) and tagged (N_t^{obs}) events, background contamination both in the total (N^{bkg}) and in the tagged sample (N^{bkg_t}) and tagging efficiencies for each centre-of-mass energy. The errors on the tagging efficiencies are statistical. In the last column the measured values of R_b are listed. The errors are statistical only

$\sqrt{s}$ (GeV)	N^{obs}	N_t^{obs}	N^{bkg}	N_t^{bkg}	Tagging efficiencies	R_b
133	850	134	138.5 ± 2.0	23.8 ± 0.4	$\varepsilon_b = 0.676 \pm 0.007$ $\varepsilon_c = 0.097 \pm 0.004$ $\varepsilon_{uds} = 0.023 \pm 0.001$	0.177 ± 0.023
161	319	45	28.2 ± 0.4	3.9 ± 0.2	$\varepsilon_b = 0.645 \pm 0.006$ $\varepsilon_c = 0.103 \pm 0.003$ $\varepsilon_{uds} = 0.031 \pm 0.001$	0.152 ± 0.035
172	266	43	38.0 ± 0.4	3.7 ± 0.1	$\varepsilon_b = 0.619 \pm 0.006$ $\varepsilon_c = 0.095 \pm 0.003$ $\varepsilon_{uds} = 0.032 \pm 0.001$	0.212 ± 0.045
183	1172	147	185.8 ± 0.9	16.6 ± 0.3	$\varepsilon_b = 0.621 \pm 0.004$ $\varepsilon_c = 0.091 \pm 0.002$ $\varepsilon_{uds} = 0.033 \pm 0.001$	0.145 ± 0.020
189	3462	486	524.3 ± 2.3	50.6 ± 0.6	$\varepsilon_b = 0.600 \pm 0.002$ $\varepsilon_c = 0.099 \pm 0.001$ $\varepsilon_{uds} = 0.044 \pm 0.001$	0.163 ± 0.013

The background includes the contribution from non-$q\bar{q}$ events and the contamination of radiative hadronic events. The radiative background decreases from 16% at 133 GeV to 4% at 189 GeV. The background due to processes other than $e^+e^- \to q\bar{q}(\gamma)$ is dominated by hadronic W decays for $\sqrt{s} \geq 161$ GeV and varies from 1% at $\sqrt{s} = 161$ GeV to 11% at 189 GeV. The background from $e^+e^- \to q\bar{q}q'\bar{q}'$ events is at the level of 1% at 189 GeV and negligible at lower centre-of-mass energies. The contribution from other processes is negligible.

The number of selected and tagged events and the background contamination both in the total and in the tagged sample for each centre-of-mass energy are shown in Table 3. The tagging efficiencies are also quoted along with their statistical errors. The b tagging efficiency decreases slightly with increasing centre-of-mass energy due to the larger non-$q\bar{q}$ background contribution. The measured values of R_b are shown in Table 3 together with their statistical errors.

The stability of the measurements has been checked by varying the cut on the b-tagging discriminant. The results of this check for the two high statistics samples at $\sqrt{s} = 183$ GeV and 189 GeV are shown in Fig. 2. No statistically significant deviation

from the R_b value obtained with the nominal cut is observed. The event-tag method used in this analysis has been cross-checked by measuring R_b using the calibration data collected each year at the Z peak. The results are found to be in good agreement with our published value [4].

4. Systematic uncertainties on R_b

The largest contribution to the systematic uncertainty on R_b comes from the description of the tracking resolution function in the Monte Carlo, since it affects the estimation of the tagging efficiencies involved in the R_b measurement. In order to study this source of systematic uncertainty, several Monte Carlo samples were reconstructed, where the parameters used to describe the resolution function have been varied according to their estimated uncertainty. The differences between the values of ε_b, ε_c and ε_{uds} obtained from these Monte Carlo samples and the nominal values shown in Table 3 have been propagated to obtain an estimation of the systematic uncertainty due to tracking resolution effects.

Another source of systematic uncertainty comes from the description in the Monte Carlo of the tracking efficiency and of the relative fraction of tracks with a given SMD hit pattern. To study this effect, the tracking efficiency has been varied in the Monte Carlo by $\pm 2\%$ and a migration of tracks at the level of 1% between the different classes has been introduced. The systematic uncertainty coming from this source has been obtained as above by propagating the variations on the flavour tagging efficiencies. The systematic uncertainties discussed above are added in quadrature to give the total systematic uncertainty due to tracking effects.

The modelling of b and c quark fragmentation and decays introduces a systematic uncertainty on R_b since the tagging efficiency for b and c quarks is obtained from Monte Carlo. Modelling uncertainties of the b-hadron properties are estimated by varying the mean value of the b-hadron energy fraction $\langle x_E(b) \rangle$, the charged decay multiplicity and the average lifetime of b-hadrons. For the estimation of ε_c an accurate knowledge of production and decay properties of the c-hadrons is important, since the
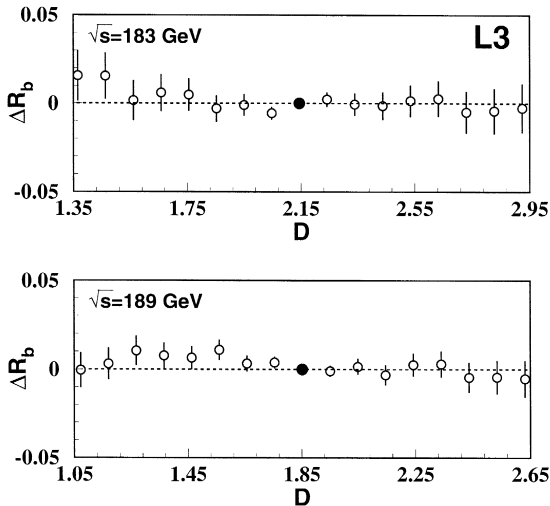

Fig. 2. Variation of R_b as a function of the cut on the b-tagging discriminant for the high statistics data samples at $\sqrt{s} = 183$ GeV and 189 GeV. The solid circles correspond to the measured values of R_b.

Table 4
Summary of systematic uncertainties on R_b due to b and c-hadron physics modelling

Source	ΔR_b				
	133 GeV	161 GeV	172 GeV	183 GeV	189 GeV
b fragmentation	0.0015	0.0014	0.0020	0.0014	0.0016
b lifetime	0.0003	0.0003	0.0004	0.0003	0.0003
b decay multiplicity	0.0010	0.0009	0.0013	0.0009	0.0011
c modelling	0.0005	0.0006	0.0006	0.0006	0.0006
total b, c physics modelling	0.0019	0.0018	0.0025	0.0018	0.0021

different species, D^0, D^+, D_s and Λ_c, have lifetimes varying in the range of 0.2 to 1.1 ps [20]. The variation of the parameters is performed following the recommendations of Ref. [21]. A breakdown of the systematic uncertainties due to the modelling of b and c-hadron physics is given in Table 4.

The error due to the finite Monte Carlo statistics has been estimated by propagating the statistical errors on ε_b, ε_c and ε_{uds}. The systematic uncertainty due to the selection of the $e^+e^- \to q\bar{q}(\gamma)$ event sample has been estimated by varying the selection cuts and taking the corresponding variation of R_b as a systematic uncertainty. The error coming from the non-$q\bar{q}$ and radiative background estimation was evaluated by varying the background fractions within their estimated uncertainties.

The various contributions to the systematic uncertainty on R_b are summarised in Table 5.

5. Measurement of A_{fb}^b

The forward–backward charge asymmetry of b quarks is measured by tagging $e^+e^- \to b\bar{b}$ events with electrons and muons with high momentum and high transverse momentum with respect to the near-

est jet. The leptons are also used to identify the charge of the b quarks. The quark direction is estimated using the event thrust axis. To enhance the b purity, the b-tagging method previously described is used.

5.1. Lepton identification and event selection

Muons are identified in the muon chamber system. The muon tracks must include track segments in at least two of the three layers of muon chambers and must point to the interaction region.

Electrons are selected in the barrel region $|\cos\theta| < 0.7$. They are identified by an energy deposit in the electromagnetic calorimeter consistent with an electromagnetic shower matching with a track in the central tracker. To reject misidentified hadrons, the energy in the hadron calorimeter behind the electromagnetic shower is required to be less than 6 GeV.

The momentum of muon candidates is required to be greater than 6 GeV, while that of the electron candidates must be greater than 3 GeV. The lepton transverse momentum, p_t, is defined with respect to the nearest jet, where the measured momentum of the lepton is not included in the jet reconstruction. If there is no jet with an energy greater than 6 GeV in

Table 5
Summary of systematic uncertainties on R_b

Source	ΔR_b				
	133 GeV	161 GeV	172 GeV	183 GeV	189 GeV
tracking effects	0.004	0.004	0.005	0.003	0.004
b, c physics modelling	0.002	0.002	0.003	0.002	0.002
MC statistics	0.003	0.002	0.003	0.001	0.001
event selection	0.002	0.002	0.002	0.002	0.002
background	0.001	0.001	0.001	0.001	0.001
total systematic uncertainty	0.005	0.005	0.007	0.004	0.005

Table 6

Fractions of events in the various categories described in the text, estimated from Monte Carlo. The corresponding asymmetry contributions used in the likelihood fit are shown in the last column

Category	Muons (%)	Electrons (%)	A_k
$b \to l$	33.20 ± 0.40	16.80 ± 0.30	A_b
$b \to c \to l$	8.20 ± 0.20	1.45 ± 0.10	$-A_b$
$b \to \bar{c} \to l$	1.80 ± 0.10	0.45 ± 0.05	A_b
$b \to J/\psi \to l$	0.40 ± 0.05		0
$b \to \tau \to l$	1.10 ± 0.09	0.70 ± 0.06	A_b
$b \to \text{fake } l$	5.70 ± 0.20	12.90 ± 0.30	A_{bckg}
$c \to l$	14.70 ± 0.35	2.10 ± 0.10	$-$
$c \to \text{fake } l$	5.50 ± 0.40	12.70 ± 0.45	$-$
$u,d,s \to l, \text{fake } l$	21.10 ± 0.25	37.20 ± 0.30	$-$
rad. background	3.80 ± 0.20	4.40 ± 0.10	$-$
WW background	4.50 ± 0.20	11.30 ± 0.45	$-$

the same hemisphere as the lepton, the p_t is calculated relative to the thrust axis of the event. The transverse momentum of the leptons must be greater than $0.7\,\text{GeV}$ to enhance the $b\bar{b}$ purity. In events containing more than one lepton candidate, only the lepton with the highest p_t is used in the asymmetry analysis. In order to further reduce the background coming from radiative $q\bar{q}$ events and W pair production, the angle α between the lepton and the event thrust axis must satisfy the requirement $|\cos\alpha| > 0.95$.

A cut in the (p_t, D) plane is applied to enhance the b purity, where D is the discriminant variable used for the measurement of R_b. The cut is defined by:

$$D > -1.8\, p_t + 2.4 \qquad (\text{muons}),$$
$$D > -0.7\, p_t + 1.6 \qquad (\text{electrons}). \qquad (4)$$

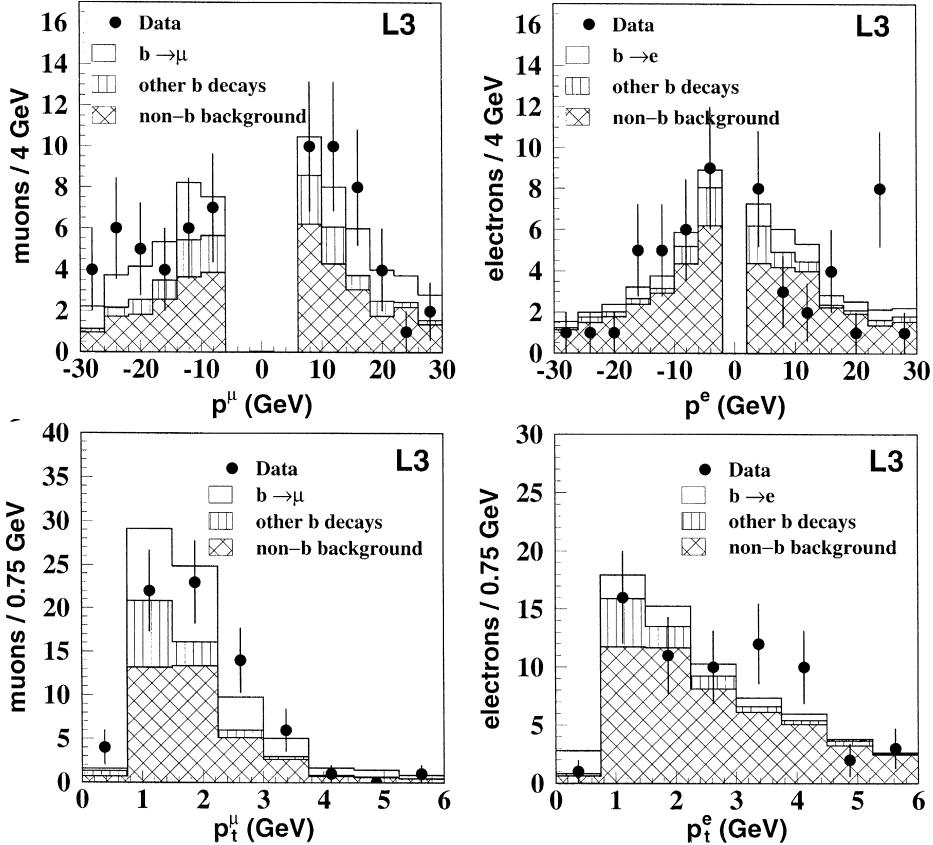These cuts were chosen as a result of an optimisation procedure.

Fig. 3. Momentum and transverse momentum distributions for selected leptons. The histograms show the estimated composition of the sample according to Table 6.

The number of prompt lepton candidates is 136, comprising 71 muon candidates and 65 electron candidates in good agreement with the Monte Carlo expectation of 139.4 events with 75.3 muons and 64.1 electrons.

Monte Carlo events are classified into eleven categories as listed in Table 6. Leptons in b events not arising from the semi-leptonic decays of categories 1 to 5 are classed as ''b → fake lepton''. This set of events consists of leptons from π and K decays, Dalitz decays and photon conversions and of misidentified hadrons. The Monte Carlo estimate of the sample composition is shown in Table 6 together with the asymmetry contribution of each event class.

The purities are 33.2% for the muon sample and 16.8% for the electron sample. The efficiencies corresponding to these purities are 21.2% and 7.6% respectively. The momentum and transverse momentum spectra for the selected muon and electron candidates together with the sample composition are shown in Fig. 3.

5.2. Asymmetry determination

The b quark scattering angle is obtained from the observable $\cos\theta_b = -q\cos\theta_T$, where the thrust direction θ_T is oriented into the hemisphere containing the lepton and q is the lepton charge. The distribution of $\cos\theta_b$ for the selected muon and electron samples is shown in Fig. 4.

Monte Carlo studies of the ''b → fake lepton'' class indicate a residual correlation between the quark charge and the observed charge, for both muons and electrons. Variations of the generator level asymmetry reveal a linear correlation with the observed asymmetry for this class of events with $A_{bckg} = (0.16 \pm 0.09) \times A_b$ for muons and $(0.25 \pm 0.08) \times A_b$ for electrons, where the errors on the factors are statistical. Variations by the statistical errors on the factors are used to estimate systematic uncertainties arising from the A_{bckg} assignment. A comparison with results obtained using a constant A_{bckg} indicate differences of 0.013 and 0.018 in the final measured asymmetries for muons and electrons, respectively.

For each lepton i in the data, the probability $f_k(i)$ to belong to each of the first six categories listed in Table 6 is determined from the number and type of Monte Carlo leptons found in the appropriate $\cos\theta_b$ bin. The asymmetry is obtained by applying a maxi-
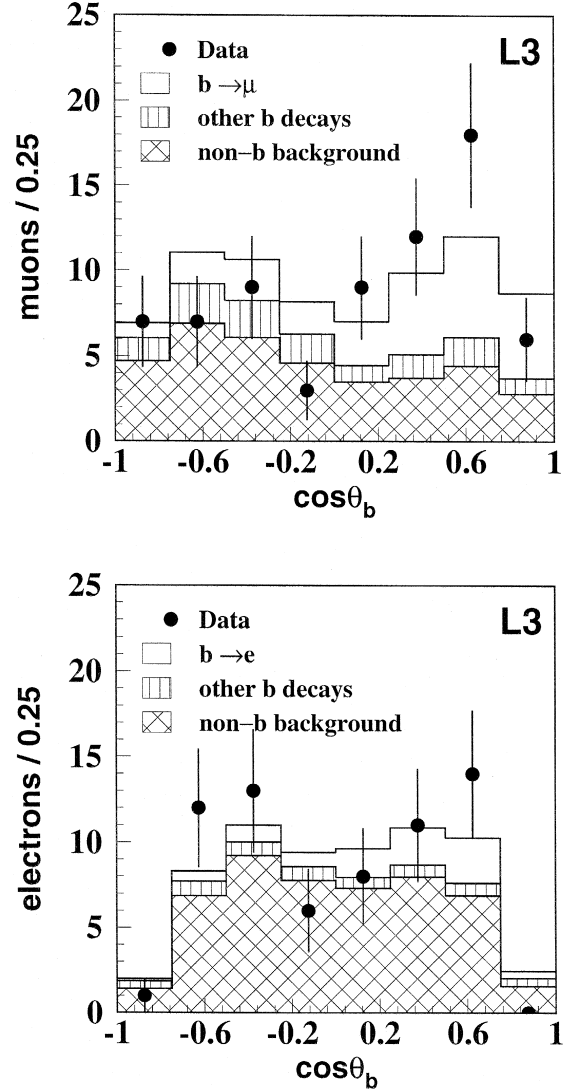
Fig. 4. Distribution of the scattering angle $\cos\theta_b = -q\cos\theta_T$ for the muon and electron samples, respectively. The histograms represent the sample composition according to Table 6.

mum-likelihood fit assuming no $B^0\bar{B}^0$ mixing. The likelihood function has the form:

$$\mathscr{L} = \frac{\prod_{i=1}^{N_{data}} \sum_{k=1}^{6} f_k(i)\left[\frac{3}{8}(1+\cos^2\theta_i) + A_k\cos\theta_i\right]}{\prod_{j=1}^{N_{MC}^{non-b}} \left(\sum_{k=1}^{6} f_k(j)\left[\frac{3}{8}(1+\cos^2\theta_j) + A_k\cos\theta_j\right]\right)^{W(j)}},$$

(5)

where A_k is the asymmetry contribution for the signal category k and $W(j)$ represents the Monte Carlo to data normalisation relevant to the Monte Carlo lepton j, obtained from the ratio of the total number of data and Monte Carlo leptons found in the corresponding $\cos\theta_b$ bin. The product over non-b Monte Carlo leptons in the denominator takes into account non-b background contributions in the data sample.

The fitted asymmetries, corrected for the charge confusion ($2.0 \pm 0.2\%$ for electrons, and $0.1 \pm 0.1\%$ for muons) and $B^0\overline{B}^0$ mixing ($\chi_B = 0.1192 \pm 0.0068$ [4,22]), are

$$A_{fb}^{b,\mu} = 0.70 \pm 0.22 \,(\text{stat.}),$$
$$A_{fb}^{b,e} = 0.39 \pm 0.34 \,(\text{stat.}). \qquad (6)$$

6. Systematic uncertainties on A_{fb}^b

The dependence of the measured asymmetry on other electroweak parameters R_b, R_c or A_{fb}^c used in the Monte Carlo modelling can be parametrised by:

$$\Delta A_{fb}^b = a(X)\,\Delta X \qquad (7)$$

where $\Delta X = X - X^{SM}$ for $X = R_b$, R_c or A_{fb}^c. The values of R_b^{SM}, R_c^{SM} and $A_{fb}^{c,SM}$ used in the Monte Carlo are given in Table 7 together with the values of the coefficients $a(X)$.

Relevant fragmentation parameters, semileptonic decay models, and branching ratios are set to their measured values and their uncertainties are used to estimate the systematic uncertainty on the asymmetry. The parameter values and variations follow the recommendations developed in Ref. [21] and are listed in Table 8 along with the corresponding systematic uncertainties on A_{fb}^b.

Table 7
Values of the Standard Model parameters R_b^{SM}, R_c^{SM} and $A_{fb}^{c,SM}$ used in the A_{fb}^b analysis and coefficients $a(X)$ giving the dependence of A_{fb}^b on them (Eq. (7))

Standard Model value	$a(X)$
$R_b^{SM} = 0.166$	-0.81
$R_c^{SM} = 0.252$	$+1.44$
$A_{fb}^{c,SM} = 0.62$	$+0.47$

Table 8
Systematic uncertainties on A_{fb}^b. The values and variations for the charge confusion correction and momentum smearing are given in the text

Contribution	Value	Variation	ΔA_{fb}^b
$x_E(b)$	0.702	± 0.008	∓ 0.004
$x_E(c)$	0.484	± 0.008	$+ 0.006$
$Br(b \to l)$	0.105	± 0.005	∓ 0.007
$Br(b \to c \to l)$	0.080	± 0.005	$+ 0.004$
$Br(b \to \bar{c} \to l)$	0.013	± 0.005	∓ 0.001
$Br(b \to \tau \to l)$	0.005	± 0.001	∓ 0.002
$Br(c \to l)$	0.098	± 0.005	$+ 0.013$
$Br(b \to J/\psi \to l)$	0.001	± 0.001	$+ 0.002$
fragmentation and branching ratios			0.017
$b \to l$ model			∓ 0.005
$c \to l$ model			$+ 0.025$
$b \to D$ model			$+ 0.003$
decay models			0.026
background fractions		$\pm 5\%$	$+ 0.024$
u, d, s background asymmetry	0.00	± 0.02	∓ 0.020
A_{bckg} asymmetry		± 0.08	∓ 0.004
background effects			0.031
p_t background description			± 0.073
lepton momentum smearing			± 0.005
charge confusion correction			∓ 0.002
mixing dependence	0.1192	0.0068	± 0.010
detector effects			0.074
total systematic uncertainty			0.087

Effects due to uncertainties in the lepton momentum resolution are estimated by smearing the muon momentum by 1% and the electron momentum by 5%. The uncertainty on the charge confusion correction is included as a contribution to the systematic uncertainty.

Table 9
Summary of results on R_b. The first error is statistical, and the second is systematic. The values predicted by the Standard Model[19] are shown in the last column

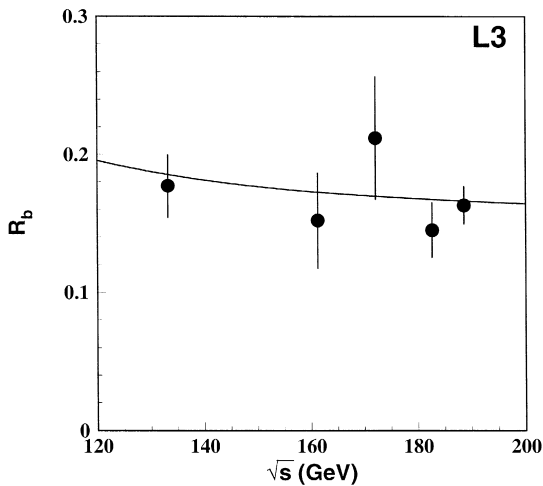| $\sqrt{s}$ (GeV)	R_b	SM expectation
133.2	$0.177 \pm 0.023 \pm 0.005$	0.185
161.3	$0.152 \pm 0.035 \pm 0.005$	0.172
172.1	$0.212 \pm 0.045 \pm 0.007$	0.169
182.7	$0.145 \pm 0.020 \pm 0.004$	0.167
188.6	$0.163 \pm 0.013 \pm 0.005$	0.166

Fig. 5. Measured values of R_b as a function of centre-of-mass energy. The curve is the Standard Model prediction [19].

A possible bias on the measured asymmetry due to the non-b background contribution is estimated by varying each background fraction by $\pm 5\%$ and the light quark asymmetry by ± 0.02. The corresponding variations in A_{fb}^b are taken as systematic uncertainties.

To study the Monte Carlo description of the p_t spectrum of the non-b background, Monte Carlo events have been compared with high statistics background-enhanced data samples. Using these data samples to constrain the shape of the p_t spectrum, Monte Carlo reweighting factors for non-b background are obtained in each p_t bin and used to modify the weights $W(j)$ in Eq. (5). Half of the change in the measured asymmetry caused by this reweighting procedure is assigned as a systematic uncertainty from the background p_t description.

The total systematic uncertainty on A_{fb}^b is given in Table 8.

7. Results

The measured values of R_b are summarised in Table 9 with their statistical and systematic errors. The measurements are compared to the Standard Model prediction in Fig. 5. At $\sqrt{s} = 189\,\text{GeV}$ the measured value of R_b is:

$$R_b = 0.163 \pm 0.013\,(\text{stat.}) \pm 0.005\,(\text{syst.})$$

to be compared with the Standard Model value [19] of 0.166.

The two measured values for $A_{fb}^{b,\mu}$ and $A_{fb}^{b,e}$ (Eq. (6)) are consistent and they are combined to give at $\sqrt{s} = 189\,\text{GeV}$:

$$A_{fb}^b = 0.61 \pm 0.18\,(\text{stat.}) \pm 0.09\,(\text{syst.})$$

to be compared with the Standard Model value [19] of 0.58.

Acknowledgements

References

[1] S.L. Glashow, Nucl. Phys. 22 (1961) 579; S. Weinberg, Phys. Rev. Lett. 19 (1967) 1264; A. Salam, Elementary Particle Theory, N. Svartholm (Ed.), Stockholm, Almquist & Wiksell, 1968, p. 367; M. Veltman, Nucl. Phys. B 7 (1968) 637; G.M. 't Hooft, Nucl. Phys. B 35 (1971) 167; G.M. 't Hooft, M. Veltman, Nucl. Phys. B 44 (1972) 189; Nucl. Phys. B 50 (1972) 318.

[2] ALEPH Collaboration, R. Barate et al., Phys. Lett. B 401 (1997) 163; ALEPH Collaboration, R. Barate et al., Phys. Lett. B 426 (1998) 217; ALEPH Collaboration, D Buskulic et al., Phys. Lett. B 384 (1996) 414.

[3] DELPHI Collaboration, P. Abreu et al., Eur. Phys. J. C 10 (1999) 415; DELPHI Collaboration, P. Abreu et al., Eur. Phys. J. C 9 (1999) 367; DELPHI Collaboration, P. Abreu et al., Eur. Phys. J. C 10 (1999) 219; DELPHI Collaboration, P. Abreu et al., Z. Phys. C 65 (1995) 569.

[4] L3 Collaboration, M. Acciarri et al., Eur. Phys. J. C 13 (1999) 47; L3 Collaboration, M. Acciarri et al., Phys. Lett. B 448 (1999) 152; L3 Collaboration, M. Acciarri et al., Phys. Lett. B 439 (1998) 225.

[5] OPAL Collaboration, G. Abbiendi et al., Eur. Phys. J. C 8 (1999) 217; OPAL Collaboration, K. Ackerstaff et al., Z. Phys. C 75 (1997) 385; OPAL Collaboration, G. Alexander et al., Z. Phys. C 73 (1997) 379; OPAL Collaboration, G. Alexander et al., Z. Phys. C 70 (1996) 357.

[6] SLD Collaboration, K. Abe et al., Phys. Rev. Lett. 80 (1998) 660.

[7] E. Eichten, K. Lane, M. Peskin, Phys. Rev. Lett. 50 (1983) 811.

[8] L3 Collaboration, B. Adeva et al., Nucl. Instr. Meth. A 289 (1990) 35; J.A. Bakken et al., Nucl. Instr. Meth. A 275 (1989) 81; O. Adriani et al., Nucl. Instr. Meth. A 302 (1991) 53; B. Adeva et al., Nucl. Instr. Meth. A 323 (1992) 109; K. Deiters et al., Nucl. Instr. Meth. A 323 (1992) 162; M. Chemarin et al., Nucl. Instr. Meth. A 349 (1994) 345; G. Basti et al., Nucl. Instr. Meth. A 374 (1996) 293; A. Adam et al., Nucl. Instr. Meth. A 383 (1996) 342.

[9] M. Acciarri et al., Nucl. Instr. Meth. A 351 (1994) 300.

[10] ALEPH Collaboration, R. Barate et al., Eur. Phys. J. C 12 (2000) 183; DELPHI Collaboration, P. Abreu et al., Eur. Phys. J. C 11 (1999) 383; OPAL Collaboration, G. Abbiendi et al., CERN-EP/99-170, submitted to Eur. Phys. J.C.

[11] L3 Collaboration, M. Acciarri et al., CERN-EP/99-181, Accepted by Phys. Lett. B.

[12] S. Catani et al., Phys. Lett. B 269 (1991) 432; S. Bethke et al., Nucl. Phys. B 370 (1992) 310.

[13] T. Sjöstrand, PYTHIA 5.7 and JETSET 7.4 Physics and Manual, CERN–TH/7112/93 (1993), revised August 1995; Comp. Phys. Comm. 82 (1994) 74.

[14] KORALZ version 4.01 is used. S. Jadach, B.F.L. Ward, Z. Wąs, Comp. Phys. Comm. 79 (1994) 503.

[15] PHOJET version 1.05 is used. R. Engel, Z. Phys. C 66 (1995) 203; R. Engel, J. Ranft, Phys. Rev. D 54 (1996) 4244.

[16] KORALW version 1.21 is used. M. Skrzypek, S. Jadach, W. Placzek, Z. Wąs, Comp. Phys. Comm. 94 (1996) 216; M. Skrzypek, S. Jadach, M. Martinez, W. Placzek, Z. Wąs, Phys. Lett. B 372 (1996) 289.

[17] F.A. Berends, R. Kleiss, R. Pittau, Nucl. Phys. B 424 (1994) 308; Nucl. Phys. B 426 (1994) 344; Nucl. Phys. (Proc. Suppl.) B 37 (1994) 163; Phys. Lett. B 335 (1994) 490; Comp. Phys. Comm. 83 (1994) 141.

[18] L3 Collaboration, M. Acciarri et al., Phys. Lett. B 411 (1997) 373.

[19] ZFITTER version 6.23 is used with default parameters except FINR = 0, INTF = 1, ISPP = −1. Moreover the physical input parameters are: Z mass = 91.1867 GeV, top quark mass = 174.1 GeV, Higgs mass = 127.0 GeV, α_s = 0.119 and $\Delta\alpha_h^{(5)}(M_Z^2) = 0.02804$. D. Bardin et al., hep-ph/9908433, submitted to Comp. Phys. Comm., http://www.ifh.de/theory/publist.html.

[20] C. Caso et al., Eur. Phys. J. C 3 (1998) 1, and 1999 off-year partial update for the 2000 edition available on the PDG WWW pp. (http://pdg.lbl.gov/).

[21] The LEP Heavy Flavour Working Group: Input Parameters for the LEP/SLD Electroweak Heavy Flavour Results for Summer 1998 Conferences, LEPHF/98-01, ALEPH Note 98-062 PHYSIC 98-027, DELPHI 98-118 PHYS 789, L3 Note 2320, OPAL Technical Note TN557, September 2, 1998, http://lepewwg.web.cern.ch/LEPEWWG/heavy/lephf9801.ps.gz.

[22] L3 Collaboration, M. Acciarri et al., Phys. Lett. B 335 (1994) 542.